

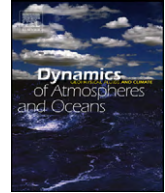


ELSEVIER

Contents lists available at ScienceDirect

Dynamics of Atmospheres and Oceans

journal homepage: www.elsevier.com/locate/dynatmoce



Short communication

Equivalent forcing depth in tropical oceans

Takeshi Doi*, Tomoki Tozuka, Toshio Yamagata

Department of Earth and Planetary Science, Graduate School of Science, The University of Tokyo, Tokyo, Japan

ARTICLE INFO

Article history:

Received 9 April 2009

Received in revised form 3 March 2010

Accepted 3 March 2010

Available online 10 March 2010

Keywords:

Equivalent forcing depth

Tropical oceans

Baroclinic mode

ABSTRACT

The forcing efficiency for the first and the second baroclinic modes by the wind stress in tropical oceans has been discussed by calculating equivalent forcing depth from annual mean, seasonal, and pentadal density profiles of the observational data. In the annual mean field, the first mode is forced preferentially in the western Pacific and the Indian Ocean, whereas the second mode is more strongly excited in the Atlantic and the eastern Pacific. This difference is mostly due to the pycnocline depth; the second mode is more dominantly forced where the pycnocline depth is shallower. We also revealed large seasonal variations of the second mode's equivalent forcing depth in the western Indian Ocean. The first mode is more dominantly forced during boreal spring and fall in the western Indian Ocean, while the second mode becomes more dominantly forced during boreal summer and winter. Those are due to seasonal variations of both the zonal wind and the pycnocline depth. Moreover, we show that the excitation of the second mode in the western Pacific increases after the late 1970s, which is associated with the decreasing trend of the zonal pycnocline gradient. Revealing the variation of the equivalent forcing depth will be useful for understanding the oceanic response to winds in tropical oceans and the improvement in the predictability of air-sea coupled climate variability in the tropics.

© 2010 Elsevier B.V. All rights reserved.

1. Introduction

The oceanic response to winds is crucial in understanding variations of the ocean circulation (Stommel, 1948). In particular, it is important to understand which vertical mode is excited most

* Corresponding author. Current address: Geophysical Fluid Dynamics Laboratory/NOAA, US Route 1, Princeton University Forrestal Campus, Princeton, NJ 08542, USA. Tel.: +1 609 452 6511.

E-mail address: Takeshi.Doi@noaa.gov (T. Doi).

efficiently by winds (Veronis and Stommel, 1956). Interannual and decadal variations of the relative importance among vertical modes are also crucial for the predictability of the El Niño–Southern Oscillation (ENSO) in the Pacific (Timmermann et al., 1999; Moon et al., 2004). Since coastal Kelvin waves originated in the tropical oceans have a potential impact on the oceanic condition of coastal regions (e.g. Sprintall et al., 2000; Li and Clarke, 2004; Florenchie et al., 2003; Iskandar et al., 2005), understanding which vertical modes are dominantly forced by winds will be useful for improving predictability of climate variations from intraseasonal to decadal time scale in both tropical and coastal regions along eastern boundaries.

Relative importance among vertical modes has been discussed in the previous literature. Evidence of the first baroclinic mode as the most efficiently forced mode in the equatorial Pacific is quite abundant (Wunsch and Gill, 1976). However, Dewitte et al. (1999), using a high-resolution ocean general circulation model (OGCM) simulation, showed that the contribution of the second baroclinic mode is larger in the eastern equatorial Pacific. At least two baroclinic modes are necessary to model successfully the equatorial thermocline depth, zonal current, and SST anomalies in both central and eastern equatorial Pacific (Giese and Harrison, 1990; Shu and Clarke, 2002). In the Atlantic, the second mode is dominantly forced at seasonal timescales (Du Penhoat and Treguier, 1985). This is consistent with the phase speed estimated from the sea surface height (SSH) anomalies observed by the TOPEX/Poseidon and ERS1/2 altimeters (Schouten et al., 2005). Also, Illig et al. (2004) revealed that the most energetic mode is the second mode at interannual timescales. These second baroclinic oceanic waves also can influence the interannual variation of the Angola Dome in the southeastern tropical Atlantic, as shown in Doi et al. (2007) by use of high-resolution OGCM outputs. In the equatorial Indian Ocean, there is a disagreement among past studies. Gent et al. (1983) showed the dominance of the second baroclinic mode. In contrast, Iskandar et al. (2005) recently have shown that the eastward propagation of intraseasonal Kelvin waves in the eastern equatorial Indian Ocean is explained by the first baroclinic mode with the phase speed of about 2.9 m s^{-1} . The latter study is in good agreement with the observation of Sprintall et al. (2000) for semiannual Kelvin waves.

We have used the equivalent forcing depths (Gill, 1982) to investigate baroclinic response of the ocean to wind forcing. The equivalent forcing depths are sometimes referred to as projection coefficients or wind-coupling coefficients, and are different from the ordinary equivalent depth (Appendix A). Although the concept of equivalent forcing depth is very interesting, unfortunately it has not been a familiar one and has not been discussed comprehensively in tropical oceans at least in our knowledge. Therefore, as a first step, we calculated the equivalent forcing depth in tropical oceans from the observational data and investigated its annual mean, seasonal variation, and pentadal variation in each basin. Although either basin-wide resonance (Cane and Moore, 1981) or local resonance (Yamagata, 1987) may affect the relative importance among the excited vertical modes for time-dependent forcing, we here concentrate on the oceanic response to the local-wind forcing.

2. Annual mean

Using the mean density profile from the World Ocean Atlas 2001 (WOA01; <http://www.nodc.noaa.gov>), we calculated equivalent forcing depths for n -th vertical mode (D_n) by:

$$D_n = \frac{H_{\text{mix}} \int_{-H}^0 A_n^2(z) dz}{\int_{-H_{\text{mix}}}^0 A_n(z) dz}, \quad (1)$$

where $A_n(z)$ is the vertical structure function, H is the bottom depth, and H_{mix} is the mixed-layer depth (Appendix A). We note that the wind stress can efficiently excite the n -th vertical mode if D_n is small. Hereafter we particularly focus our attention on the first two gravest modes. Fig. 1a shows the value of $D_1/(D_1 + D_2)$ in the global equatorial ocean. In the area where the value is above 0.5, the second mode is more dominantly forced by the wind stress than the first mode. The second mode is more dominantly forced in the whole equatorial Atlantic, as shown in the previous works (Du Penhoat and Treguier, 1985; Illig et al., 2004). Interestingly, the dominantly forced mode changes within the Pacific;

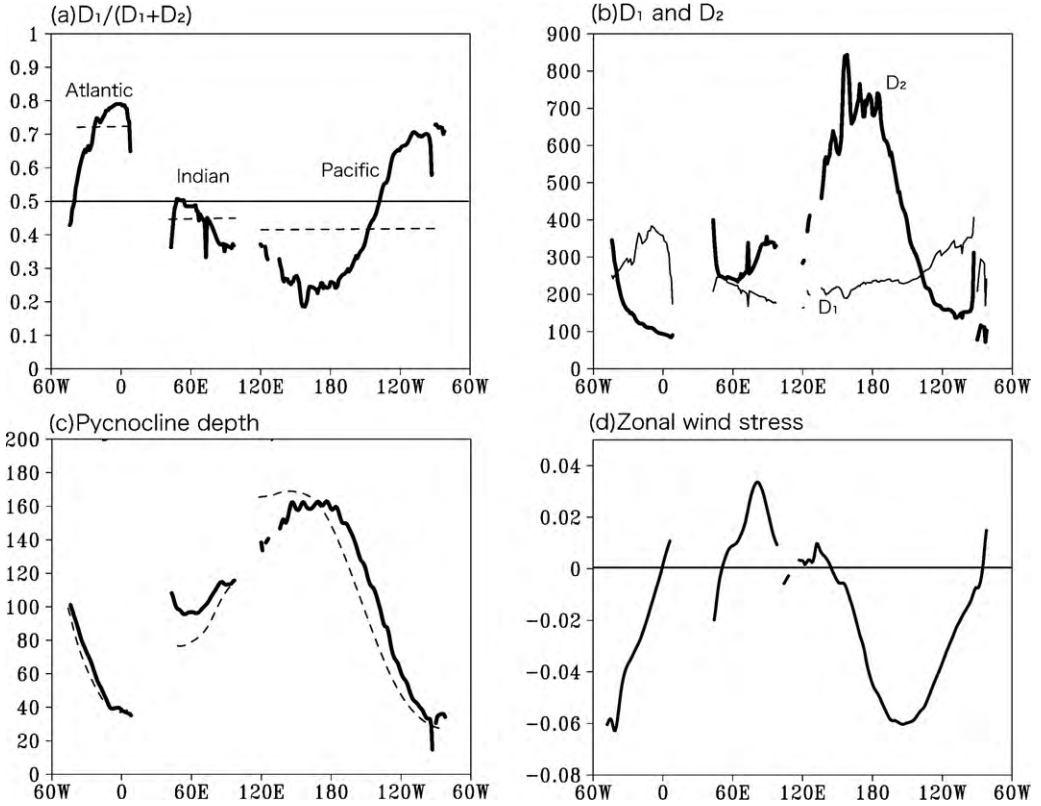


Fig. 1. (a) Value of $D_1/(D_1 + D_2)$ along the equator (solid line). The dash lines show the averages in each basin. Value above 0.5 means that the second mode is forced more dominantly by winds than the first mode. (b) Values of D_1 (thin line) and D_2 (thick line) (in m). (c) Pycnocline depth, which is defined by a depth of $1024.5\ kg\ m^{-3}$, from the WOA01 (solid line) and the estimation by Eq. (2) (dash line) (in m). (d) Zonal wind stress along the equator from the QSCAT wind data (in $N\ m^{-2}$).

the first mode is more dominantly forced in the western and central Pacific while the second mode is more dominantly forced in the eastern Pacific. Therefore, we need to pay attention not only to first baroclinic modes, but also second baroclinic modes for understanding the oceanic variation in the equatorial Pacific, as discussed by Giese and Harrison, 1990; Shu and Clarke, 2002. The present results, however, are different from that of Fukumori et al. (1998), who compared the relative magnitude of two baroclinic modes using an OGCM. They showed that the first mode is more efficiently forced in the whole equatorial Pacific. This discrepancy maybe due to the coarse vertical resolution (only three points above pycnocline depth in their model) and thus an unrealistic diffused pycnocline, which favors the excitation of the first mode. As the value of $D_1/(D_1 + D_2)$ in the western and central Indian Ocean is close to 0.5, both the first and the second vertical modes are almost equally forced there, but the first mode becomes more dominantly forced to the east. It is consistent with Iskandar et al. (2005), who showed that the first baroclinic Kelvin waves play important roles on the intraseasonal variation in the eastern equatorial Indian Ocean by use of high-resolution OGCM outputs.

The zonal variation of $D_1/(D_1 + D_2)$ depends strongly on the variation of D_2 more than that of D_1 , as shown in Fig. 1b. The variance of D_2 is 2.5 times larger than that of D_1 . The variation of D_2 can be explained mostly by the zonal variation of depths of $1024.5\ kg\ m^{-3}$ potential density surface (Fig. 1c), which lies near centers of pycnocline. The correlation coefficient between the zonal distribution of D_2 and that of pycnocline depth is higher than 0.9. Assuming a simple shallow-water model, the pycnocline depth is simply estimated by zonally integrating the mean zonal winds stress from the

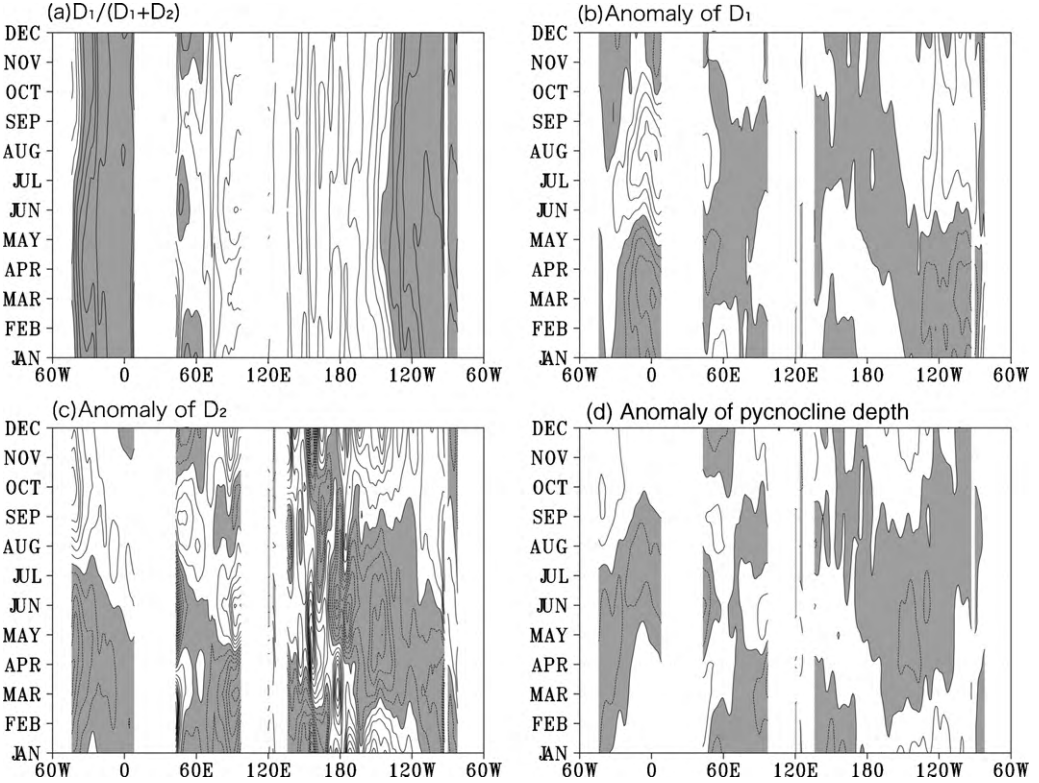


Fig. 2. (a) Seasonal march in the value of $D_1/(D_1 + D_2)$ along the equator. Values above 0.5 are shaded. Contour interval is 0.05. (b) Seasonal deviations of D_1 from the annual mean (in m). Negative values are shaded, and Contour interval is 20 m. (c) As in (b), but for D_2 . (d) Seasonal deviations of pycnocline depth from the annual mean (in m). Negative values are shaded, and contour interval is 10 m.

eastern boundary:

$$h(x) = H_{\text{east}} + \frac{1}{\rho_0 H_{\text{upper}} g'} \int_{x'=\text{east}}^x T_{\text{surf}}^x(x') dx', \quad (2)$$

where h is the pycnocline depth, ρ_0 is the reference density, H_{upper} is upper layer depth, H_{east} is upper layer depth at the eastern boundary, g' is the reduced gravity acceleration, and T_{surf}^x is zonal wind stress. We used the QSCAT wind data (Kubota et al., 2002) for zonal wind stress and estimated the pycnocline depth (Fig. 1d). It is in good agreement with the estimation from the WOA01 (Fig. 1c). The differences of the basin size and zonal wind stress seem to be important factors for the difference of the pycnocline depth. If we focus on the zonal mean values of $D_1/(D_1 + D_2)$ averaged over each basin (Fig. 1a), the second mode is more efficiently forced in the Atlantic, while the first mode is more dominantly forced in both the Pacific and the Indian Oceans. This is also explained by the difference of the pycnocline depth estimated by Eq. (2) averaged over each basin. The difference between the Atlantic and the Pacific is remarkable. Since the zonal wind stress averaged over each basin does not have so big differences between the Atlantic and the Pacific, the zonal basin size must be crucial for the difference of equivalent forcing depth.

3. Seasonal variation

Fig. 2a shows seasonal variations of $D_1/(D_1 + D_2)$ calculated from the monthly climatology of the WOA01 data. Although the dominantly forced mode remains the same throughout the year over the

most part, the western Indian Ocean shows annual march conspicuously. The first mode is more dominantly forced during boreal spring and fall in the western Indian Ocean, while the second mode becomes more dominantly forced during boreal summer and winter. This seasonal variation is mainly due to the seasonal variation of D_2 associated with the seasonal variation of the pycnocline depth (Fig. 2b–d), as similar to annual mean feature in the previous section. Because the pycnocline depth is deeper during boreal spring and fall in the western Indian Ocean, D_2 becomes larger and thus the excitation of the second mode becomes weaker there.

Therefore, the season when the baroclinic Kelvin wave is forced by winds is important to discuss the oceanic response especially in the equatorial Indian Ocean. This may also explain the disagreement between the present study and Gent et al. (1983). They showed that the second vertical mode is most strongly excited throughout the year for the whole equatorial Indian Ocean, using the density profile observed at 53°E during May and June. As is clear from Fig. 2a, the second mode is more strongly forced at 53°E during May and June. Furthermore, the phase speed of the semiannual Kelvin wave during the monsoon transition periods of April and October is comparable with that of the first baroclinic mode (Sprintall et al., 2000). This is again consistent with our result that the first mode is forced dominantly during these seasons.

4. Pentadal variation

Fig. 3a shows the pentadal variation of $D_1/(D_1 + D_2)$ calculated from the pentadal anomaly data of the WOA01 (e.g. Levitus et al., 2005; Boyer et al., 2005). Although this dataset would be suffered from lack of systematic ocean measurements, we believe that calculating the long-term variation of the equivalent forcing depth by use of this dataset is worthwhile as a first step. The order of relative importance of excitation remains the same throughout the past 40 years over the most part, except for the western Indian Ocean. In this area, the most dominantly forced mode can be changed between the first mode and the second mode. The first mode is dominantly forced during 1960–1968 and 1981–1985, while the second mode is dominantly forced during 1955–1959, 1969–1980 and 1986–present averaged over 57°–60°E. We need to be careful in discussing the oceanic response to winds in this area. This pentadal variation is expected to affect on climate variation in the equatorial Indian Ocean.

Focusing on D_2 , the pentadal variation in the western Pacific is rather large compared to the other oceans (Fig. 3b). D_2 in the western Pacific decrease after the late 1970s, which is reliable above 99% significance level based on Mann–Kendall rank statistic and t -test, and D_2 in the late 1990s is 300 m smaller than the late 1970s. This means that the excitation of second mode in the western Pacific increase after the late 1970s. This result seems to be very important for understanding the changed amplitude and period of ENSO after the late 1970s (Moon et al., 2004), as the remote forcing by changes in wind stress in the western Pacific are important in pycnocline depth in the eastern Pacific (Busalacchi and O'Brien, 1981). The pentadal variation of D_2 can be also explained by the pycnocline depth (Fig. 3c). The pycnocline in the western Pacific becomes shallower and that in the eastern Pacific becomes deeper after the late 1970s. This can be explained by the weakness of the trade wind in the Pacific after the late 1970s (Fig. 3d), as shown in Vecchi et al. (2006). This is consistent with the Intergovernment Panel on Climate Change (IPCC) report of Cubasch et al. (2001), who concluded that the future mean Pacific climate base state could more resemble an El Niño-like state, i.e. a slackened west to east SST gradient associated with the eastward shift of precipitation. Our result supports the previous works (Shu and Clarke, 2002; Moon et al., 2004), but our new viewpoint is to discuss those from the equivalent forcing depth calculated using the observational data, not an assimilation data nor a model output.

5. Summary

We have discussed relative importance of the first and the second baroclinic oceanic response to winds in the three tropical oceans from a viewpoint of equivalent forcing depth calculated by use of the WOA01 dataset. In the annual mean, the first mode is forced preferentially in the western Pacific and the Indian Ocean, whereas the second mode is forced in the Atlantic and the eastern Pacific. The difference is mostly due to the pycnocline depth; the second mode is more efficiently forced where

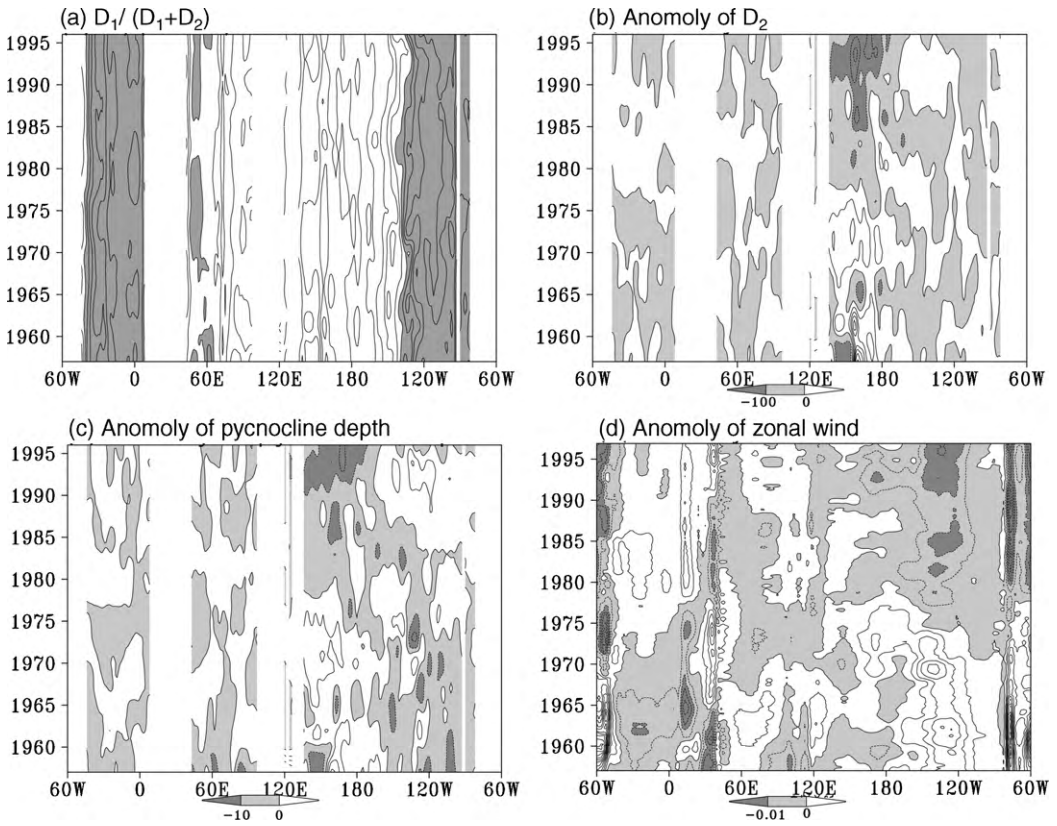


Fig. 3. (a) Pentadal march in the value of $D_1/(D_1 + D_2)$ along the equator. Values above 0.5 are shaded. Contour interval is 0.05. (b) Pentadal deviations of D_2 from the annual mean (in m). Negative values are shown by shading, and Contour interval is 100 m. (c) Pentadal deviations of pycnocline depth from the annual mean (in m). Negative values are shown by shading, and contour interval is 10 m. (d) Pentadal deviations of zonal wind stress (in N m^{-2}) from the annual mean by use of the NCEP/NCAR reanalysis data (Kalney et al., 1996). Westerly wind anomalies are shown by shading, and contour interval is 0.01 N m^{-2} .

the pycnocline is shallower. This pycnocline depth is explained using the balance between horizontal pressure gradient and zonal wind stress.

Large seasonal variations of D_2 are revealed in the western Indian Ocean. The first mode is more dominantly forced during boreal spring and fall in the western Indian Ocean, while the second mode becomes more dominantly forced during boreal summer and winter. Therefore, we need to be careful in discussing the oceanic response to winds in this area. Also, pentadal variation of D_2 in the western Pacific is large compared to the other basin; the excitation of second mode in the western Pacific increase after the late 1970s. It may be associated with the decreasing trend of the zonal pycnocline gradient or the mixed-layer trend. Further studies using assimilation datasets or model outputs are necessary to investigate the trend in the excitation efficiency of the second modes relative to the first modes more deeply and this actual influence on the climate mode in the Pacific.

Acknowledgements

The present research is supported by the Japan Society for Promotion of Science (JSPS) through both Grant-in-Aid for Scientific Research B (50091400). Also, the first author is supported by the Research Fellowship of the JSPS for Young Scientists (208479).

Appendix A. Equivalent forcing depth

The linear equations including the wind forcing term are:

$$\frac{\partial u}{\partial t} - fv = -\rho_0^{-1} \frac{\partial P}{\partial x} + \rho_0^{-1} \frac{\partial X^x}{\partial z} \tag{A1}$$

$$\frac{\partial v}{\partial t} + fu = -\rho_0^{-1} \frac{\partial P}{\partial y} + \rho_0^{-1} \frac{\partial X^y}{\partial z} \tag{A2}$$

$$\frac{\partial P}{\partial z} = -\rho'g \tag{A3}$$

$$\frac{\partial u}{\partial x} + \frac{\partial v}{\partial y} + \frac{\partial w}{\partial z} = 0 \tag{A4}$$

$$\frac{\partial \rho'}{\partial t} + w \frac{\partial \bar{\rho}}{\partial z} = 0, \tag{A5}$$

where $u, v,$ and w are the zonal, meridional, and vertical velocity, respectively, P and ρ' are the pressure and potential density perturbation from a mean state $\bar{\rho}$, g is the acceleration due to gravity, ρ_0 is the reference density, f is the Coriolis parameter, X^x and X^y are the zonal and meridional wind forcing term, respectively. Eqs. (A3) and (A5) reduce to

$$\frac{1}{\rho_0} \frac{\partial^2 P}{\partial t \partial z} = -N^2 w \tag{A6}$$

$$N^2 = -\frac{g}{\rho_0} \frac{\partial \bar{\rho}}{\partial z}, \tag{A7}$$

where N is the Brunt–Väisälä frequency, which is calculated from the vertical profile of potential density of the WOA01 data in a central difference scheme. The horizontal velocity and the pressure are then written as:

$$(u, v, p) = \sum_{n=0}^{\infty} (\tilde{u}_n(x, y, t), \tilde{v}_n(x, y, t), \tilde{p}_n(x, y, t)) A_n(z). \tag{A8}$$

Using the continuity equation:

$$\frac{\partial w}{\partial z} = -\frac{\partial u}{\partial x} - \frac{\partial v}{\partial y} = \sum_{n=0}^{\infty} \tilde{w}_n(x, y, t) A_n(z), \tag{A9}$$

the vertical velocity is written as:

$$w = \sum_{n=0}^{\infty} \tilde{w}_n(x, y, t) S_n(z), \quad \frac{\partial S_n(z)}{\partial z} = A_n(z), \tag{A10}$$

where S_n is the vertical structure functions of vertical velocity. Substituting (A8) and (A10) into (A6), we obtain

$$\frac{d}{dz} \left(\frac{1}{N^2} \frac{dA_n}{dz} \right) + \frac{1}{C_n^2} A_n = 0. \tag{A11}$$

The vertical structure function $A_n(z)$ is a solution of an eigenvalue problem of Eq. (A11) with boundary conditions: $\int_{-H}^0 A_n dz = 0$. Here, H is the bottom depth, and the eigenvalue C_n is the phase speed for the mode n . The A_n forms a set of orthogonal functions and are normalized by $A_n(0) = 1$ for all n . We can solve this eigenvalue problem numerically from the vertical density profile.

In the same manner of Eq. (A8), the wind forcing term can be written as:

$$\rho_0^{-1} \left(\frac{\partial X^x}{\partial z} \right) = \rho_0^{-1} \sum_{n=0}^{\infty} (\tilde{\tau}_n^x(x, y, t) A_n(z)). \tag{A12}$$

Multiplying both sides by $A_n(z)$ and integrating over the whole depth using orthogonality property, we obtain

$$\tilde{\tau}_n^x \int_{-H}^0 \frac{A_n^2}{\rho_0} dz = \int_{-H}^0 \frac{1}{\rho_0} \frac{\partial X^x}{\partial z} A_n dz. \quad (\text{A13})$$

Here, we assume a linear variation of wind stress over the mixed-layer thickness H_{mix} , which is calculated as the depth at which the potential density becomes 0.125 kg m^{-3} larger than the surface density in this study. Then, Eq. (A13) simplifies to

$$\tilde{\tau}_n^x \int_{-H}^0 \frac{A_n^2(z)}{\rho_0} dz = \frac{X_{\text{surf}}^x}{H_{\text{mix}}} \int_{-H_{\text{mix}}}^0 \frac{A_n(z)}{\rho_0} dz, \quad (\text{A14})$$

where X_{surf}^x is zonal wind stress on surface. Therefore, we have

$$D_n = \frac{H_{\text{mix}} \int_{-H}^0 A_n^2(z) dz}{\int_{-H_{\text{mix}}}^0 A_n(z) dz} \quad (\text{A15})$$

$$(\tilde{\tau}_n^x, \tilde{\tau}_n^y) = \frac{(X_{\text{surf}}^x, X_{\text{surf}}^y)}{D_n}, \quad (\text{A16})$$

where D_n is called a equivalent forcing depth (Gill, 1982). Wind stress excites efficiently the vertical mode for which the equivalent forcing depth is small. An equivalent forcing depth should not be confused with an ordinary equivalent depth, the latter is related to the baroclinic wave speed (Wunsch and Gill, 1976). Also, we note that equivalent forcing depths are sometimes calculated simply by $\int_{-H}^0 A_n^2(z) dz$ without the actual value of the mixed-layer depth (e.g. Du Penhoat and Treguier, 1985), because $H_{\text{mix}} / \int_{-H_{\text{mix}}}^0 A_n(z) dz$ is almost unity under the condition that $A_n(0) = 1$ for all n . We calculated D_n also by using this simplified formula and confirmed almost the same results.

References

- Busalacchi, A.J., O'Brien, J.J., 1981. Interannual variability of the Equatorial Pacific in the 1960s. *J. Geophys. Res.* 86, 10901–10907.
- Boyer, T.P., et al., 2005. Linear trends in salinity for the World Ocean, 1955–1998. *Geophys. Res. Lett.* 32, doi:10.1029/2004GL021791.
- Cane, M.A., Moore, D.W., 1981. A note on low-frequency equatorial ocean to periodic forcing. *J. Phys. Oceanogr.* 11, 1578–1584.
- Cubasch, U., et al., 2001. Projections of future climate change. In: Houghton, J.T., et al. (Eds.), *Climate Change 2001: The Scientific Basis*. Cambridge University Press, pp. 527–582.
- Dewitte, B., Reverdin, G., Maes, C., 1999. Vertical structure of an OGCM simulation of the equatorial Pacific Ocean in 1985–94. *J. Phys. Oceanogr.* 29, 1542–1570.
- Doi, T., Tozuka, T., Sasaki, H., Masumoto, Y., Yamagata, T., 2007. Seasonal and interannual variation of oceanic conditions in the Angola Dome. *J. Phys. Oceanogr.* 37, 2698–2713.
- Du Penhoat, Y., Treguier, A.M., 1985. The seasonal linear response of the tropical Atlantic Ocean. *J. Phys. Oceanogr.* 15, 316–329.
- Florenchie, P., Lutjeharms, J.R.E., Reason, C.J.C., Masson, S., Rouault, M., 2003. The source of Benguela Niños in the South Atlantic Ocean. *Geophys. Res. Lett.* 30, doi:10.1029/2003GL017172.
- Fukumori, I., Raghunath, R., Fu, L.L., 1998. Nature of global large-scale sea level variability in relation to atmospheric forcing: a modeling study. *J. Geophys. Res.* 103, 5493–5512.
- Gent, P.G., O'Neill, K., Cane, M.A., 1983. A model of the semiannual oscillation in the equatorial Indian Ocean. *J. Phys. Oceanogr.* 13, 2148–2160.
- Giese, B.S., Harrison, D.E., 1990. Aspects of the Kelvin wave response to episodic wind forcing. *J. Geophys. Res.* 95, 7289–7312.
- Gill, A., 1982. *Dynamics of Atmospheres and Oceans*. Academic Press, UK.
- Illig, S., Dewitte, B., Ayoub, N., Du Penhoat, Y., Reverdin, G., De Mey, P., Bonjean, F., Lagerloef, G.S.E., 2004. Interannual long equatorial waves in the tropical Atlantic from a high-resolution ocean general circulation model experiment in 1981–2000. *J. Geophys. Res.* 109, doi:10.1029/2003JC001771.
- Iskandar, I., Mardiansyah, W., Masumoto, Y., Yamagata, T., 2005. Intraseasonal Kelvin waves along the southern coast of Sumatra and Java. *J. Geophys. Res.* 110, doi:10.1029/2004JC002508.
- Kalney, E., et al., 1996. The NCEP/NCAR 40-year reanalysis project. *Bull. Am. Meteorol. Soc.* 77, 437–471.
- Kubota, M., Iwasaka, N., Kizu, S., Konda, M., Kutsuwada, K., 2002. Japanese ocean flux data sets with use of remote sensing observations (J-OFURO). *J. Oceanogr.* 58, 213–225.
- Levitus, S., Antonov, J., Boyer, T., 2005. Warming of the world ocean, 1955–2003. *Geophys. Res. Lett.* 32, doi:10.1029/2004GL021592.
- Li, J., Clarke, A.J., 2004. Coastline direction, interannual flow, and the strong El Niño currents along Australia's nearly zonal southern coast. *J. Phys. Oceanogr.* 34, 2373–2381.

- Moon, B.-K., Yeh, S.-W., Dewitte, B., Jhun, J.-G., Kang, I.-S., Kirtman, B.P., 2004. Vertical structure variability in the equatorial Pacific before and after the Pacific climate shift of the 1970s. *Geophys. Res. Lett.* 31, doi:10.1029/2003GL018829.
- Schouten, M.W., Matano, R.P., Strub, T.P., 2005. A description of the seasonal cycle of the equatorial Atlantic from altimeter data. *Deep Sea. Res.* 52, 477–493.
- Shu, L., Clarke, A.J., 2002. Using an ocean model to examine ENSO dynamics. *J. Phys. Oceanogr.* 32, 903–923.
- Sprintall, J., Gordon, A., Murtugudde, L.R., Susanto, R.D., 2000. A semiannual Indian Ocean forced Kelvin wave observed in the Indonesian seas in May 1997. *J. Geophys. Res.* 105, 17,217–17230.
- Stommel, H., 1948. The westward intensification of wind-driven ocean currents. *Trans. Am. Geophys. Union* 29, 202–206.
- Timmermann, A., Oberhuber, J., Bacher, A., Esch, M., Latif, M., Roeckner, E., 1999. Increased El Niño frequency in a climate model forced by future greenhouse warming. *Nature* 398, 694–697.
- Vecchi, G.A., Soden, B.J., Wittenberg, A.T., Held, I.M., Leetmaa, A., Harrison, M.J., 2006. Weakening of tropical Pacific atmospheric circulation due to anthropogenic forcing. *Nature* 441, 73–76.
- Veronis, G., Stommel, H., 1956. The action of variable wind stresses on a stratified ocean. *J. Mar. Res.* 15, 43–75.
- Wunsch, C., Gill, A.E., 1976. Observations of equatorially trapped waves in Pacific sea level variations. *Deep Sea Res.* 23, 371–390.
- Yamagata, T., 1987. A simple moist model relevant to the origin of intraseasonal disturbances in the tropics. *J. Meteorol. Soc. Jpn.* 65, 153–165.